UC Berkeley
UC Berkeley Previously Published Works

Title
Magnetic and structural properties of the iron oxychalcogenides La2O2Fe2OM2(M=S,Se)

Permalink
https://escholarship.org/uc/item/9f7791t6

Journal
Physical Review B, 99(2)

ISSN
2469-9950

Authors
Freelon, B
Yamani, Z
Swainson, Ian
et al.

Publication Date
2019

DOI
10.1103/physrevb.99.024109

Peer reviewed

eScholarship.org Powered by the California Digital Library
University of California

arXiv:1801.00342v1 [cond-mat.str-el] 31 Dec 2017

Magnetic and Structural Properties of the Iron Oxychalcogenides $La_2O_2Fe_2OM_2$ (M= S, Se)

B. Freelon,[1*] Z. Yamani,[2] Ian Swainson,[3] R. Flauca,[2] Yu Hao Liu,[4] L. Craco,[5] M. S. Laad,[6] Meng Wang,[7] Jiaqi Chen,[8] R. J. Birgeneau,[7,9,10] and Minghu Fang[8*]

[1] *Department of Physics, University of Louisville, Louisville, KY 40208, USA*

[2] *Canadian Nuclear Laboratories, Chalk River Laboratories, Chalk River, ON, K0J 1J0, Canada*

[3] *Physics Section, International Atomic Energy Agency, Vienna International Centre, PO Box 100, 1400 Vienna, Austria*

[4] *Department of Materials Science and Engineering, University of Illinois Urbana Champaign, Urbana, Illinois, 61801*

[5] *Instituto de Fisica, Universidade Federal de Mato Grosso, 78060-900, Cuiaba, MT, Brazil*

[6] *The Institute of Mathematical Sciences, C.I.T. Campus, Chennai 600 113, India*

[7] *Department of Physics, University of California, Berkeley, CA 94720, USA*

[8] *Department of Physics, Zhejiang University, Hangzhou 310027, P. R. China*

[9] *Materials Science Division, Lawrence Berkeley National Laboratory, Berkeley, California 94720, USA*

[10] *Department of Materials Science and Engineering, University of California, Berkeley, California 94720, USA*

(Dated: January 3, 2018)

Abstract

We present the results of structural and magnetic phase comparisons of the iron oxychalcogenides $La_2O_2Fe_2OM_2$ (M = S, Se). Elastic neutron scattering reveals that M = S and Se have similar nuclear structures at room and low temperatures. Both materials obtain antiferromagnetic ordering at a Neel temperature T_N 90.1 ± 0.16 K and 107.2 ± 0.06 K for M= Se and S, respectively. The magnetic arrangements of M = S, Se are obtained through Rietveld refinement and we present the first direct comparison of magnetic structural analysis for these materials. We find the order parameter exponent β to be 0.129 ± 0.006 for M = Se and 0.133 ± 0.007 for M = S. Each of these values is near the Ising symmetry value of 1/8. This suggest that although lattice and electronic structural modifications result from chalcogen exchange, the nature of the magnetic interactions is similar in these materials.

PACS numbers: 71.27.+a, 25.40.Dn, 78.70.Nx,

* byron.freelon@louisville.edu

I. INTRODUCTION

Iron oxychalcogenides are currently being studied [1–3] because of their structural similarity to iron-based high-transition temperature T_c superconductors (HTSC) such as iron pnictides (FePn) and iron chalcogenides (FeCh). Attention has been given to iron oxychalcogenides since they are known to exhibit band narrowing induced Mott localization in their non-magnetically ordered phase. [4] In a close parallel to the cuprates, this strongly correlated electronic feature has garnered interest from investigators seeking to discover new iron-based materials in which high-T_c superconductivity might be obtained by doping the Mott insulating state. [5–7]

A particularly intriguing iron-oxychalcogenide system is $RE_2O_2TM_2OM_2$ (RE = rare-earth element, TM = transition-metal element and M = (S or Se). The crystal structure (see Fig. 1) contains tetragonally ordered Fe planes that are similar to iron pnictides because chalcogens alternate above and below the iron atoms. In addition, Oxygen atoms are contained in the RE layers.[5, 8] While similar to the FePn, the iron oxychalcogenides are structurally reminiscent of the cuprate HTSCs since there are distinct TM-O and RE-O regions. An important feature of the Fe planes is the presence of a center Oxygen O(2) atom that serves to increase the Fe unit cell (u.c.) relative to that of the iron-pnictides and -chalcogenides. It has been suggested that the increased Fe u.c. leads to narrowing of the iron bands. [9]

Iron oxychalcogenides were first reported to have insulating properties by Mayer. [8] These materials exhibit strongly correlated Mott insulating behavior while offering tunability of their electronic properties near a metal-insulator transition (MIT). Importantly, Zhu *et. al.*, using local density to dynamical mean-field theory (LDA + DMFT) predicted [5] Mott insulating behavior and band narrowing of $La_2O_2Fe_2O(S, Se)_2$. Resonant inelastic x-ray scattering (RIXS) and soft x-ray absorption spectroscopy confirmed [10] the presence of Mott insulating bands and iron band narrowing. In that same study, realistic mulit-orbital LDA + DMFT calculations suggested the presence of a novel Mott-Kondo insulating state that might support HTSC arising from a strange-metal state near a quantum critical point. It was shown that the undoped iron oxychalcogenide insulator $Na_2Fe_2OSe_2$ is a true multi-orbital Mott insulator, and that the doping-induced MIT is a manifestation of a selective Mott type, where the interplay between multi-orbital correlations and one-electron band

narrowing is important. Reminiscent of underdoped high-T_c cuprates, carrier localization in $Na_2Fe_2OSe_2$ was found to persist upon hole doping because the chemical potential lies in a gap structure with almost vanishing density of states. On the other hand, in remarkable contrast, electron-doping drives an orbital-selective metallic phase with coexisting pseudogapped (Mott-localized) and itinerant carriers.

These contrasting behaviors in a single system stem from drastic reconstruction of electronic states with distinct orbital character at low energies. This reveals that iron oxychalcogenides fit well in the class of Fe-based systems that exhibit behavior based on orbital-selective phases. [11] The nature and extent of orbital selectivity, in hole- and electron-doped cases, are expected to play an important role in determining the nature and symmetry of the superconducting state in Mott insulators. The diversity of pairing states in iron- based systems, by now appreciated [11] to be a consequence of their multi-orbital nature, may be further exposed by examining whether iron oxychalcogenides can be driven into superconductivity through the appropriate application of pressure or chemical doping. [4]

To date, the study of the normal paramagnetic (PM) and antiferromagnetic (AFM) states of FeSC (both pnictides and chalcogenides) has indicated that these materials fall into the bad-metal category. This is due to the development of a strongly renormalized lattice coherence scale, driven by the increased influence of electronic correlations as the temperature is reduced. The scale is further reduced by structural induced bare, one-particle band narrowing in the case of iron oxychalcogenides systems. In Mott insulators, sizable electronic correlations drives new physical effects upon doping (electron or hole) and other external perturbations. [12] They can induce a pseudogap regime as in the $Na_2Fe_2OSe_2$ system referred to above, where the chemical potential lies in an energy region of vanishing electronic states, [13] or orbital-selective incoherent states, naturally yielding co-existent insulating and bad metallic states as in cuprates or iron-pnictides. [14–16] In an effort to study how materials can be driven toward insulator-to-metal transitions, iron oxychalcogenides are intriguing. They can be tuned, by transition-metal or chalcogen substitution[5], across an MIT in order to produce novel electronic and magnetic phases at low temperature. In fact, the substitution of S and Se has been shown to alter the character of electronic partial density of states in this material class. [5, 10] Other studies have examined the electrical properties of the doped analogs [17] and atomically substituted Fe oxychalcogenides.

These fascinating properties have contributed to studies on a range of oxychalcogenides

including $RE_2O_2TM_2O(Ch)_2$ where TM = Co, Mn, Fe and $Fe_{1-x}Mn_x$ and *Ch* are the chalogens S and Se. [18] [5, 19–23] In addition, new compounds, $A_2F_2TM_2O(Ch)_2$ where A = (Ba, Sr) have been the subject of recent investigation. [24] These materials were shown to order antiferromagnetically; the material was proposed to be an example of a frustrated AFM checkerboard spin lattice. [24] β-$La_2O_2(Fe_{1-x}Mn_x)_2O(S, Se)_2$ and $Ce_2O_2FeSe_2$ [25–27] $Na_2Fe_2OSe_2$ also contains a $[Fe_2OSe_2]$ unit, albeit separated by alternating double layers of Na^+, as found in FeO*Ch*. $Na_2Fe_2OSe_2$ exhibits the onset of AFM ordering at 73 K and 2D short-range magnetic correlation well above T_N. [28] Craco *et. al.* predicted orbital-selective Mott behavior [4] in the electronic behavior of $Na_2Fe_2OSe_2$ and further suggested that charge doping or external pressure would induce the simultaneous occurrence of Mott insulating and coherent charge carrier behaviors.

Landsgesell investigated the effects of F-doping in $La_2O_{3-x}F_xFe_2Se_2$ (x from 0.0 to 0.5) using neutron diffraction and magnetic bulk measurements. [7] With increasing x, the size of the crystallographic unit cell decreases as well as the amplitude of the ordered magnetic moments, while the configuration of the magnetic order and the development of the resistivity on cooling remains unchanged. [7] Doping via the substitution of Mn for Fe in $La_2O_2Fe_{1-x}Mn_xOSe_2$ did not lead to observable HTSC; however, several different AFM phases were identified over the broad doping range of x = 0.1 to 0.9. [20] [23]

In this work, we present the results of a neutron diffraction study aimed at comparing the structural and magnetic properties of the iron oxychalcogenides $La_2O_2Fe_2OS_2$ and $La_2O_2Fe_2OSe_2$. Our focus is on powder materials since single-crystalline samples remain difficult to produce. To the best of our knowledge, there have been no reports of single crystalline $La_2O_2Fe_2O(S, Se)_2$. We employ neutron powder diffraction (NPD) to measure the nuclear and magnetic Bragg scattering intensity as a function of temperature and we examine the structural distinctions between the two parent compounds at room and low temperatures. Section II gives an overview of the materials and the synthesis while Section III provides experimental details of the neutron measurements. Section IV gives the results of structural and magnetic measurements of M=(S, Se). In addition, we discuss the magnetic structure and the magnetic order parameter behavior. Section V provides a discussion of our findings relative to other oxychalcogenides reports in the literature. Finally, our results are discussed in the context of theoretical findings that have been reported on $La_2O_2Fe_2O(S, Se)_2$ systems.

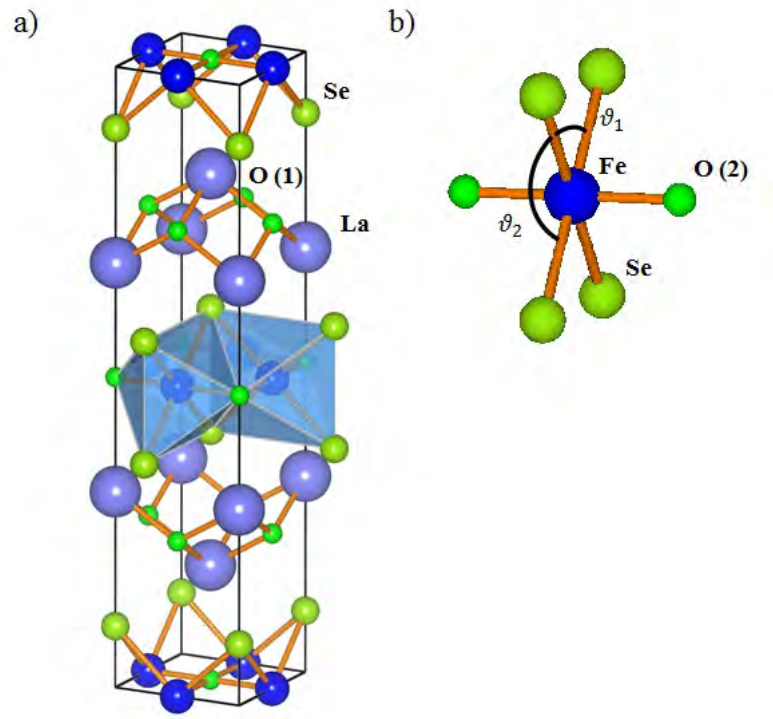

FIG. 1. (Color online) The crystal structure of $La_2O_2Fe_2O(S,Se)_2$ is shown in (a). The coordination geometry an Fe atom is shown in (b). The angles θ_1 and θ_2 are described in the text.

II. MATERIALS AND SYNTHESIS

The atomic structure (see Fig. 1 (a)) of $La_2O_2Fe_2O(S,\ Se)_2$ crystallizes in the space group $I4/mmm$ (No. 139). [8] $La_2O_2Fe_2O(S,\ Se)_2$ are insulators which contain anti-CuO_2-type square, plane-like layers. $La_2O_2Fe_2O(S,\ Se)_2$ consist of $[La_2O_2]^{2+}$ layers and $[Fe_2O]^{2+}$ layers that are separated by $(S,\ Se)^{2-}$ anions. The Fe^{2+} cations are linked through two in-plane Oxygen O(2) anions as well as four out-of- plane (S^{2-}, Se^{2-}) anions. The Fe atoms are tetrahedrally coordinated with (S, Se) atoms that are located alternatingly, above or below, the center of the Fe-O plaquettes; therefore, the Fe-M layers are not flat. They form a face-sharing octahedral unit $[Fe_2O(S,Se)_2]^{2-}$. [19]

The samples studied here $La_2O_2Fe_2(S,Se)_2$ have nominal compositions and were prepared by a conventional solid-state reaction method using high purity La_2O_3, S, Se and Fe powders as starting materials. The powders were mixed in the stoichiometric ratios and carefully

ground. Subsequently, the powders were pressed into pellets and then heated in an evacuated quartz tube at 1030°C for 3 days; this process was repeated three times. The samples were confirmed to be of a single phase by the laboratory X-ray powder diffraction measurements. [8]

III. EXPERIMENTAL

Neutron powder diffraction (NPD) experiments were performed using the C2 high-resolution diffractometer at the Canadian Neutron Beam Centre in Chalk River, Ontario. Room temperature measurements were conducted with approximately 3 g of finely ground powder of both $La_2O_2Fe_2S_2$ and $La_2O_2Fe_2Se_2$. The samples were contained in vanadium cannisters sealed with indium gaskets under an atmosphere of He exchange gas. The low temperature NPD measurements were conducted using the same cannisters. All handling of the powders was performed inside a He glovebox. The C2 diffractometer is equipped with an 800 wire position sensitive detector covering a range of 80 degrees. Data were collected in the angular range from 5° to 117° 2θ using a Si (5 3 1) monochromator at a wavelength λ of 1.33 $\mathring{A}$. Because λ is similar in scale as the atomic spacing, the incident neutrons can be Bragg diffracted by nuclear positions. Neutrons have zero-charge and a fermionic $S = 1/2$, the resulting magnetic dipole moment of the neutron interacts with unpaired electrons to reveal magnetic ordering in solid materials. Rietveld analysis of the nuclear diffraction data, conducted using the FullProf [29] program suite, estimated the samples to contain less than 1.2% and 1.3% of impurity phases in $La_2O_2Fe_2(S,Se)_2$, respectively.

Resistivity versus temperature data for M = S and Se have been published in Refs. [5] and [10]. $\mathbf{M}$ is defined as the magnetization per unit volume and $\mathbf{H}$ is the applied magnetic field (1 T in our measurement setup). The magnetic susceptibility $d\mathbf{M}/d\mathbf{H}$ as a function of temperature is shown in Fig. 2. The data were collected on powder samples with $H = 1$ T during warming using a Magnetic Properties Measurement System (MPMS) manufactured by Quantum Design, Inc. The susceptibility data are similar to what is expected from 2D AFM samples except that there are pronounced Curie tails at low temperatures. This could indicate the presence of a small concentration of paramagnetic impurities. The Curie tails were not fitted since they do not affect the susceptibility curves in the Neel regions.

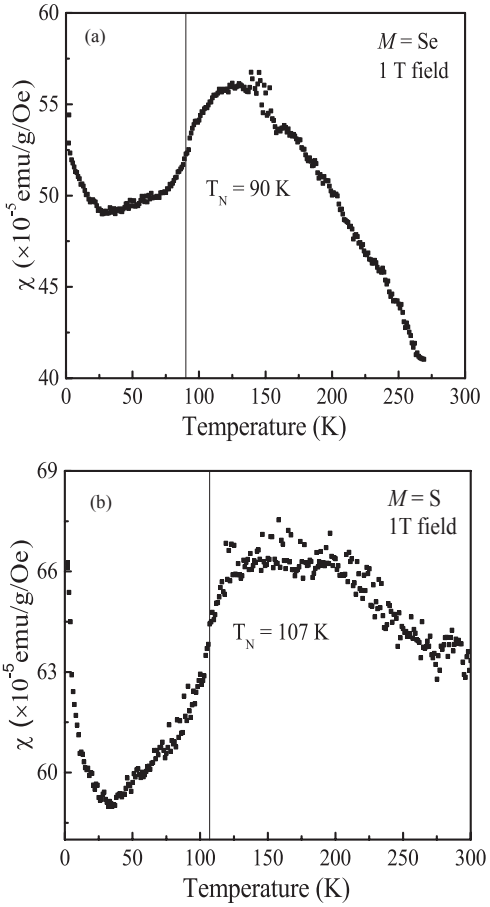

FIG. 2. (Color online) (a) The magnetic susceptibility of $La_2OFe_2O_2M_2$ a) M=Se and b) M=S.

IV. RESULTS

A. Structural Comparison: M = S, Se

Fig. 3 (a) and (b) shows the results of Rietveld structural refinement of M= S at (a) 280 K and (b) low temperature (4 K). The crystal structure refinement of the powder neutron diffraction data was carried out using the FullProf package, with the use of its internal tables for scattering lengths. These data are consistent with previous reports on M = Se. [30] Based upon the refinement, the symmetry and orientation of the magnetic moments can be assigned to a $I4/mmm$ symmetry for M = S and Se. Overall, the powder diffraction data indicate that these materials are isostructural. A direct comparison of the Rietveld refinement parameters of M= S, Se is given in Table I. Fe unit cell volume of M=

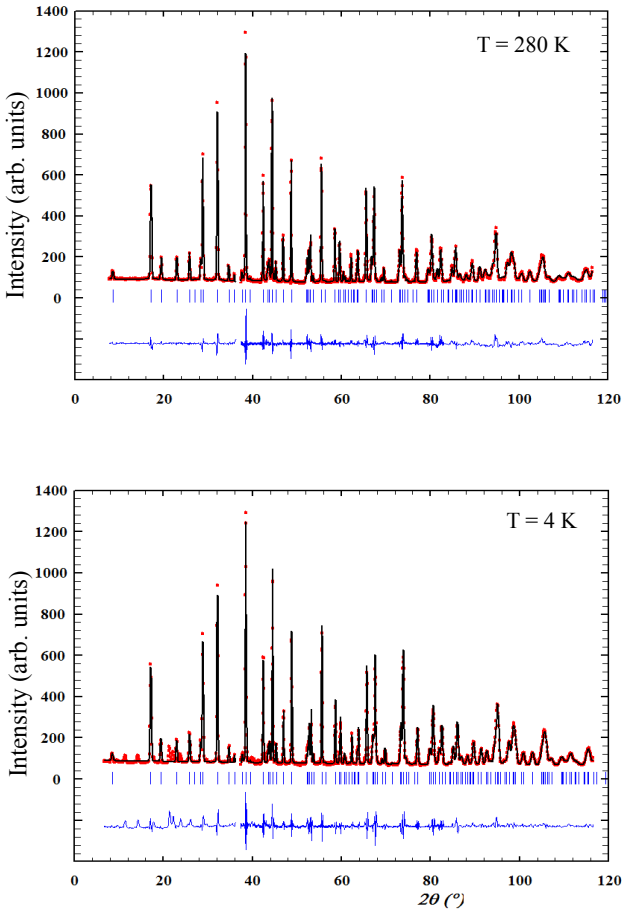

FIG. 3. (Color online) Rietveld refinement profiles using (a) 280 K and (b) low-temperature, 4 K, data for $La_2O_2Fe_2OS_2$ collected using the C2 diffractometer with wavelength λ =1.33 $\AA$. The data were refined using the space group $I4/mmm$. Observed and calculated patterns are shown in red and black, respectively, with the difference profile (blue) and nuclear Bragg peak positions shown as blue given vertical tick marks.

Se is larger than that of M= S. This is reasonable given that the ionic radius of sulfur (100 pm) is smaller than selenium (115 pm). The lattice parameters of $La_2O_2Fe_2OS_2$ (a =4.04539$\AA$, c = 17.9036$\AA$) are smaller than those of $La_2O_2Fe_2OSe_2$ (a =4.0877$\AA$, c = 18.6005$\AA$). Compared to the Fe-Fe atomic distances d_{Fe-Fe} values reported in LaFeOAs, the interatomic distances we obtained (in Table II) are larger by 1.2 % and nearly 1.1%

	$La_2OFe_2O_2Se_2$	$La_2OFe_2O_2S_2$
a [Å]	4.08778(5)	4.04539(5)
c [Å]	18.6005(3)	17.9036(3)
V[$Å^3$]	310.816(8)	292.997(8)
$4e$ La(c)	0.1843(1)	0.1811(1)
$4e$ $M(c)$	0.0964(1)	0.0933(3)
La B(Å)	0.21(5)	0.30(4)
Fe B(Å)	0.46(3)	0.42(4)
O(1) B(Å)	0.44(5)	0.40(4)
O(2) B(Å)	0.91(8)	0.89(7)
M B(Å)	0.38(4)	0.26(8)

TABLE I. Refined parameters for $La_2OFe_2O_2Se_2$ $La_2OFe_2O_2S_2$ at 280 K.

$La_2O_2Fe_2OSe_2$				$La_2O_2Fe_2OS_2$			
Length	[Å][b]	Bond Angle	[°]	Length	[Å]	Bond Angle	[°]
d_{Fe-Fe}	2.89050(3)	Fe-O-Fe (2)	90.00	d_{Fe-Fe}	2.85813(0)	Fe-O-Fe (2)	90.00
d_{Fe-O2}	2.04389(3)	Fe-Se-Fe	64.086	d_{Fe-O2}	2.02100(0)	Fe-S-Fe	64.919
d_{Fe-Se}	2.72400(4)	Se-Fe-Se	97.237	d_{Fe-S}	2.66264(0)	S-Fe-S	98.755
d_{La-O1}[e]	2.38013(3)	La-O-La (1)	118.348	d_{La-O1}	2.33787(0)	La-O-La (1)	119.642
d_{La-Se}[e]	3.31832(4)	La-O-La (2)	—	d_{La-S}	3.26261(0)	La-O-La (2)	—

TABLE II. Interatomic distances and angles of $La_2O_2Fe_2O(S, Se)_2$ at 280 K.

for M= Se and S, respectively. Bond angles and atomic distances, extracted from Rietveld refinement parameters, are tabulated for comparison of M= S and Se (see Table II). Rietveld analysis yielded measurements for the bond angles subtended by Se-Fe-Se and S-Fe-S. These bonds define the distortion in the (TMM_4) squares contained in the Fe_2OS_4 and Fe_2OSe_4 octahedra ($c.f.$ Figure 1(a)), respectively. Here we list the angles θ_1 and θ_2 (Figure 1(b)) for M = S and Se along with other oxychalcogenides. Specifically, $La_2O_2Fe_2OS_2$, 98.7° and 81.3°; $La_2O_2Fe_2OSe_2$, 97.2° and 82.8°; $Nd_2O_2Fe_2OSe_2$, 96.1° and 83.9° [31]; $La_2O_2Co_2OSe_2$,

$La_2O_2Fe_2OSe_2$					$La_2O_2Fe_2OS_2$				
Atom	Site	x	y	z	Atom	Site	x	y	z
La	4e	0.5000	0.5000	0.1844	**La**	4e	0.5000	0.5000	0.18105
Fe	4c	0.5000	0.0000	0.0000	**Fe**	4c	0.5000	0.0000	0.0000
Se	4e	0.0000	0.0000	0.0968	**S**	4c	0.0000	0.0000	0.0933
O1	4d	0.5000	0.0000	0.2500	**O1**	4d	0.5000	0.0000	0.2500
O2	2b	0.5000	0.5000	0.0000	**O2**	2b	0.5000	0.5000	0.0000

TABLE III. Atomic positions of $La_2O_2Fe_2O(S, Se)_2$ at 280 K extracted from refined parameters.

98.7° and 81.3° [32]; $Sr_2Ti_2F_2OAs_2$, 96.3° and 83.7°; $Sr_2Ti_2F_2OSb_2$, 91.0° and 89.0° [33]; $Sr_2Fe_2F_2OS_2$, 100.2° and 79.8°; $Ba_2Fe_2F_2OS_2$, 102.2° and 77.8°; $Sr_2Fe_2F_2OSe_2$, 97.2° and 82.8°. [24] A comparison of the θ_1 values for M = S, Se indicate that the S atoms are closer to the iron plane than Se chalcogens.

The Fe ion is 6-coordinated with two oxygen and 4 M = (S, Se) ions to form $[FeO_2M_4]$ octahedra possessing the D_{2h} point symmetry. These octahedra are face sharing (*c.f.* Fig. 1(a)) such that the shared face is intersected by the Fe-Fe nearest-neighbor line-of-sight. For completeness Table III presents the atomic position of constituents of $La_2O_2Fe_2O(S, Se)_2$.

Our low-temperature, high-resolution, M = (S, Se) powder diffraction data does not contain pattern changes or structural Bragg peak splittings that would indicate the occurrence of a thermally driven structural phase transition. Therefore, we do not observe the emergence of an atomic arrangement with lower symmetry as a function of temperature. This is consistent with results reported in the literature for M = Se. [30] While Free *et. al.* did not observe a structural phase transition, those authors noticed subtle temperature-dependent lattice behavior and atomic displacement parameter U_{33} trends in $La_2O_2Fe_2OSe_2$. [30] It was suggested that these features were only weak indications a lowering of lattice symmetry. It has been proposed that the absence of a structural phase transition is due to the reduction of magnetostructural coupling in $La_2O_2Fe_2O(S,Se)_2$ caused by structural disordering. [30]

B. Magnetic Comparison: M= S, Se

Upon cooling, extraneous intensity appeared in the diffraction profiles of M = S and Se. These peaks were assigned a magnetic origin on the basis of their temperature dependence and the complete Rietveld refinement of the diffraction patterns. The Se end member has been well-characterized by Free and Evans [30] and we initially followed their approach by verifying that the AFM3 model provided the best fit to the magnetic structure of $La_2O_2Fe_2OSe_2$. We used the SARAh suite of programs [34] to analyze the representations and provide the basis vectors for refinement with FullProf. [29, 35] In close similarity to what was described previously for M = Se, the magnetic cell of M = S is commensurate and is doubled in a and c with respect to the structural cell. The magnetic ordering in $La_2O_2Fe_2OS_2$ is associated with an ordering vector$\mathbf{k} = (1/2, 0, 1/2)$, and the single Fe site on $\{1/2, 0, 0\}$ in the nuclear $I4/mmm$ cell is described by two distinct orbits governing the two $\{1/2, 0, 0\}$ and $\{0, 1/2, 0\}$ Fe sites that are independent in the magnetically ordered state. In Figure 4 the low angle region of the powder diffractograms of $La_2O_2Fe_2OS_2$ and 3 K and 290 K. The data are presented such that magnetic Bragg peaks $\mathbf{Q}_M = (-101), (002)$ and (-103) are seen (blue label) to develop at low-temperatures while the structural Bragg peaks are present (black) for both high- and low-temperatures.

In order to understand the magnetic ordering, the symmetry of the magnetic structure was determined using a refinement of the magnetic intensity pattern employing FullProf. There are two independent Fe sites for both $La_2O_2Fe_2O(S, Se)_2$. The propagation vector was determined to be $\mathbf{k} = (1/2, 0, 1/2)$. By performing a full Rietveld refinement and analysis of the neutron powder diffraction data, the ordered Fe^{2+} moment of $La_2O_2Fe_2OS_2$ was determined to be 2.32(4) μ_B at 4 K; for $La_2O_2Fe_2OSe_2$ a range of values from 2.8 to 3.50(5) μ_B has been reported. [36] We then found that the AFM3 model provided good fits for the structure of M = S. The magnetic ground state is composed of the Fe ions in a high spin, non-collinear antiferromagnetically ordered state.

C. Magnetic Order Parameter Critical Behavior

To determine the thermal dependence of the magnetic ordering behavior of M = (S, Se), the intensity of the magnetic Bragg peak $\mathbf{Q}$ = (-103) was measured over a temperature

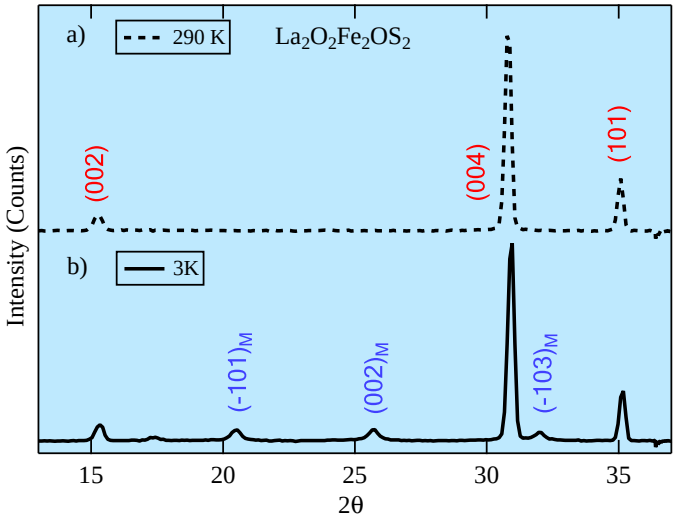

FIG. 4. (Color online) The neutron powder diffraction data for $La_2OFe_2O_2S_2$ is shown for a) 3 K and b) 290 K. Red (purple) labels indicate the (HKL) indices of the structural (magnetic) Bragg diffraction peaks.

range of 300 K to 4 K in each material. The peak intensity can be used as a measure of the magnetic order parameter squared ϕ^2. The square of the magnetic order parameters of $La_2O_2Fe_2O(S, Se)_2$ are plotted in Fig. 5. $La_2O_2Fe_2O(S,Se)_2$ peak intensity data was fitted to the power-law functional form $\phi^2(T/T_N) = (1 - T/T_N)^{2\beta_{Fe}}$. [37] β_{Fe}, the critical exponent, and T_N, the Nèel temperature, served as adjustable fit parameters. Fits were applied over the temperature range $0.05 \leq T/T_N \leq 1$ and yielded values for β_{Fe} and T_N of 0.129 ± 0.006 and $90.1(9) \pm 0.16$ K for M = Se and 0.133 ± 0.007 and $107.2(6) \pm 0.06$ K in the case of M = S. These extracted values of β_{Fe} are close to those reported for M = Se in Ref. [30]. Furthermore, the β_{Fe} for both M = S and Se are close to the Ising critical exponent β_{Ising} value of 1/8. This result indicates that the magnetic phase transitions in $La_2O_2Fe_2OS_2$ and $La_2O_2Fe_2OSe_2$ may be weakly first order. These critical exponent values also suggest that there are 2D Ising-like spin fluctuations near the critical point. The similarity of the critical exponents is further indication that the magnetic phases of $La_2O_2Fe_2OS_2$ and $La_2O_2Fe_2OSe_2$ arise from similar magnetic interaction geometries.

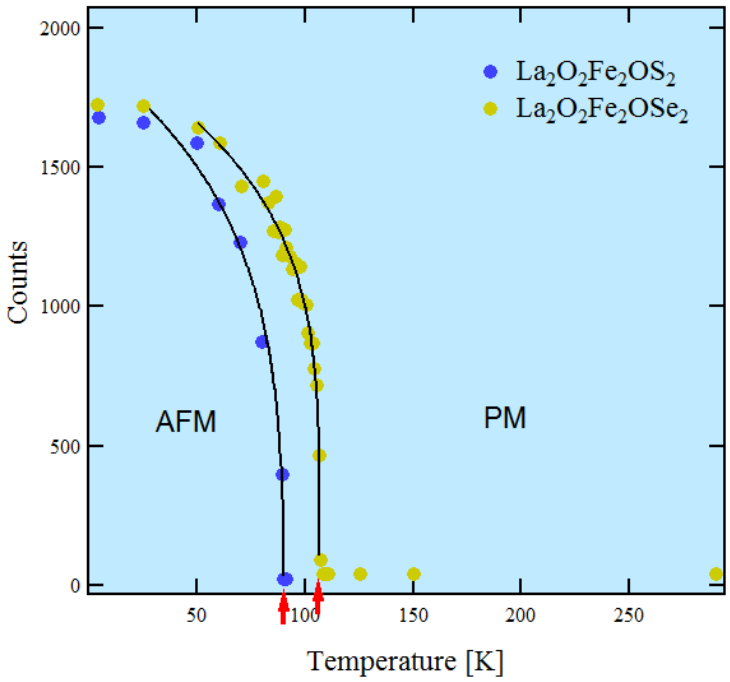

FIG. 5. (Color online) The magnetic order parameter is shown at the (1, 0, 3) magnetic Bragg reflection. The peak intensity measured at $\mathbf{Q}$ = (1, 0, 3), plotted for both $La_2O_2Fe_2O(S,Se)_2$, is used as a measure of the magnetic order parameter ϕ^2.

V. DISCUSSION

A. Structural

The first issue to be addressed is the status of symmetry lowering signatures in the low temperature diffraction data of both M = S and Se. The absence of clear splittings of structural peaks, suggestive of a lowering of lattice symmetry, can be contemplated in comparison to the iron pnictides, which actually undergo a structural phase transition from tetragonal to orthorhombic symmetry at a structural transition temperature T_S. We did not observe a structural phase transition for M = Se, neither did M = S diffraction data provide any indication of a change of lattice symmetry. This is consistent with the results of Free *et. al.* [30]; however, they [30] suggested the possibility that subtle behavior of the atomic displacement parameter U_{33} might be very weak evidence for a lowering of symmetry in M = S and Se. The pursuit of a more detailed study of the local (short-range) structure of $La_2O_2Fe_2O(S,Se)_2$ may be warranted in order to determine whether there is any localized

structural arrangement as a function of temperature. Recently, a pulsed neutron scattering study of the local structure of $La_2O_2Fe_2OSe_2$ was conducted by extracting atomic position deviations from radial distribution function data. [38] No local structure change from the low-temperature $I/4mmm$ symmetry was observed in these experiments. Both Fuwa [31] and Free [30] suggested that the absence of structural phase transitions might be due to the lack of magnetostriction or magnetoelastic coupling in $La_2O_2Fe_2OSe_2$. [4, 39] The nature of such couplings is an area of interest that warrants further explorations in these iron oxychalcogenides.

B. Magnetic

In order to discuss the magnetic structure results obtained from $La_2O_2Fe_2O(S,Se)_2$, we summarize the most prominent description of the spin interactions in RE-$O_2Fe_2OM_2$ materials. Several spin interaction labeling conventions can be found in the literature on $La_2O_2Fe_2OSe_2$; table IV lists them. We adopt the convention used in Refs. [5], [30] and [36]. The spin Hamiltonian for $La_2O_2Fe_2O(S,Se)_2$ has been modeled by Zhu *et. al* [5] using three interactions J_1, J_2 and J_2'. J_1 has several contributions: (a) a face-sharing 64° interaction between Fe-Se-Fe (b) an Fe-O-Fe 90° interaction and (c) possibly an iron nearest neighbor (NN) contribution. J_2 is a next nearest-neighbor (NNN) interaction that consists of a 98° edge-sharing term involving of Fe-Se-Fe contributions from two buckled Se atoms (iii) J_2' is a NN, 180° Fe-O-Fe interaction between the corner-sharing octahedra. Fig. 6 provides a schematic description of these interactions.

Using the interaction (J_1, J_2, J_2') labeling, Zhu *et. al.* employed a generalized gradient approximation (GGA) + Coulomb energy U calculation [5] in order to determine that the magnetic ground state of $La_2O_2Fe_2OSe_2$ should obtain either the AFM1 or the AFM6 (*c.f.* Fig. 6 in Ref. [30]) configuration depending on the value of U. By contrast, Free and Evans reported that elastic neutron scattering results indicated [30] that the magnetic moments of $La_2O_2Fe_2OSe_2$ should order in the AFM3 (see Fig. 7(a)) frustrated, collinear configuration similar to $Fe_{1.086}Te$. At variance with this finding, McCabe *et. al.* concluded that inelastic neutron scattering (INS) results on $La_2O_2Fe_2OSe_2$ are consistent with a multi-component, non-collinear 2-k magnetic structure shown in Fig. 7(b). The 2-k structure is made up of 2 orthogonal stripes within the Fe_2OM_2 layers. While the AFM3 configuration provided good

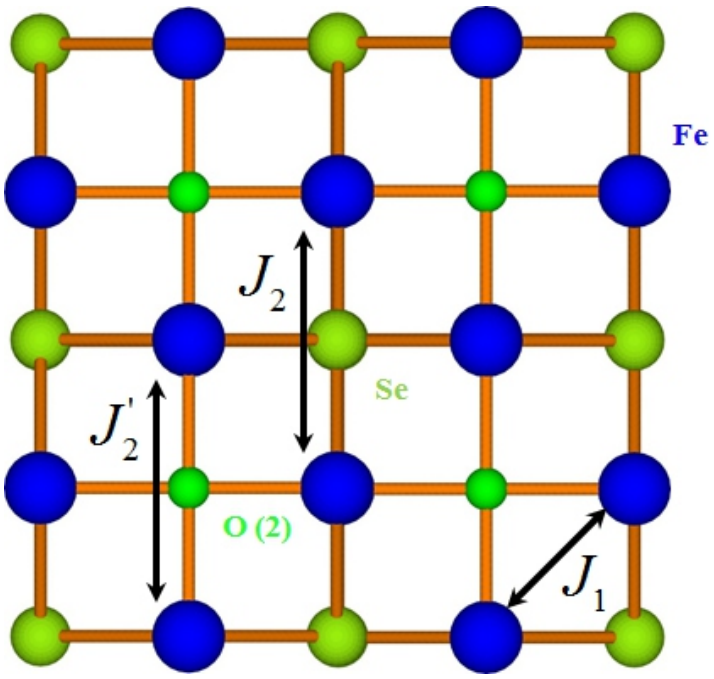

FIG. 6. (Color online) Spin interactions J_1, J_2 and J_2' used in modeling the magnetic behavior of $La_2O_2Fe_2O(S,Se)_2$. These are the principle spin interactions contained in the $Fe_2O(S, Se)_2$ layer. The details regarding each exchange constant are given within the text.

fits to our M = S and Se NPD data, as noted [36], neutron powder diffraction can not distinguish between the various AFM models that have been proposed for $La_2O_2Fe_2OSe_2$. Therefore the report of consistency between INS data and the 2-k magnetic structure provided important insights given that details on the production of single-crystalline $La_2O_2Fe_2O(S, Se)_2$ remain unpublished. In addition to neutron scattering experiments, nuclear magnetic resonance (NMR) measurements by Gunther *et. al.* were interpreted [40] to suggest that the 2-k model is the appropriate description of the M = Se.

Magnetic frustration has been addressed in $La_2O_2Fe_2OSe_2$ and other iron oxychalcogenides. Some amount of frustration in $La_2O_2Fe_2O(S, Se)_2$ is to be expected given that there are FM (J_2) and AFM (J_2') interactions associated with the FeOM_2 layer. These competing interactions, in addition to magnetocrystalline anisotropy, create a frustrated spin environment in which the FeOM_2 layer has three principal competing magnetic interactions J_1, J_2 and J_2'. [41] In contrast to the AFM3 collinear, frustrated model of Ref. [30], McCabe *et. al.* suggested the 2-k $La_2O_2Fe_2OSe_2$ structure to be weakly frustrated due to the magnetic configuration being collectively stabilized by the AFM J_2' and FM J_2 interactions

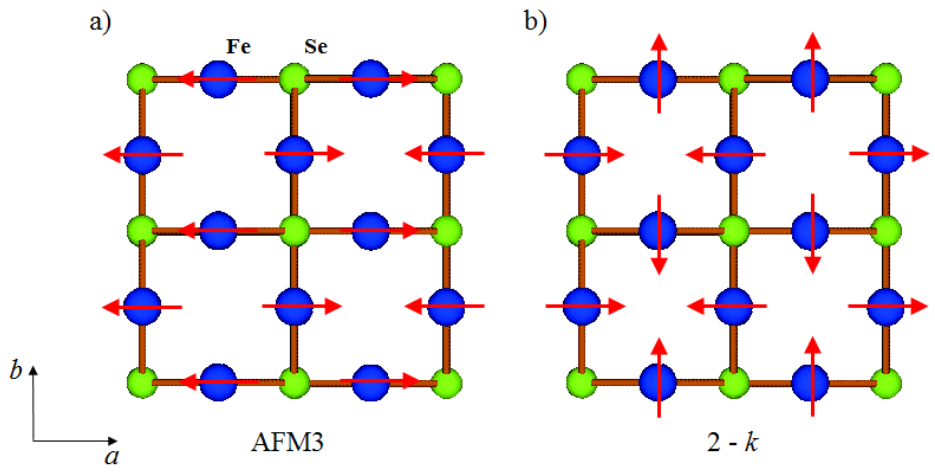

FIG. 7. (Color online) The (a) collinear AFM3 and (b) non-collinear 2-k magnetic structure models for $La_2O_2Fe_2OSe_2$.

as well as the magnetocrystalline anisotropy. Those authors reported that both the magnetic frustration and the exchange coupling are weak in $La_2O_2Fe_2OSe_2$ compared to other iron oxychalcogenides. Even though the extent of frustration in $La_2O_2Fe_2OSe_2$ is not fully understood, it is still possible to compare the magnetic frustration of M = S and Se. As seen above, structural refinements yielded a smaller bond angle Fe-M-Fe in M = S than for M = Se. This is an indication that the M = S NNN distances are smaller and, therefore, have increased magnetic exchange. Furthermore, the NN exchange of M = S is increased relative to that of M = Se. It has been proposed [31] that the NNN AFM interaction J_2' in $Nd_2O_2Fe_2OSe_2$ is due to the Goodenough-Kanamori rule. [42] This proposal might explain the difference in Neel temperatures observed for M = S and M = Se.

TABLE IV. Magnetic Interaction Naming Conventions

Interaction	Description	Geomtery	Ref. [5, 30, 36],[a]	[20, 24, 41]
NNN	Fe-O-Fe	180°	J_2'	J_1
NN	TM-TM	in-plane	J_1	J_3
NNN	TM-Ch-TM	$\sim$ 90°	J_2	J_2

Notes: The (next) nearest neighbor interactions are $(N)NN$

[a] This work.

Several spin Hamiltonians have been introduced in order to address the magnetic behavior of materials thought to be within strong coupling limit *e.g.* iron oxychalcogenides and iron alkaline selenides $A_{0.8}Fe_{1.6}Se_2 \rightarrow A_2Fe_4Se_5$ (referred to as "245s" where A = Rb, Cs, K and Tl). [43–46] Unlike the iron pnictides, the increased electron correlation of the iron chalcogenides and iron alkaline selenides leads to narrower iron bandwidths. Consequently, despite the absolute value of the Hunds coupling being similar to that of the pnictides ($J_H \sim 0.7$ eV), its role is more pronounced, resulting in a larger spin $S = 2$. Importantly, INS experiments [36] have yielded $S = 2$ for $La_2O_2Fe_2OSe_2$ and $RbS_{0.8}FeS_{1.5}S_2$ [47].

Finally, we address the absence of $La_2O_2Fe_2O(S,Se)_2$ structural phase transitions in the context of the magnetic behavior of these materials. The lack of a structural phase transition occurring in close proximity to the formation of antiferromagnetism is at variance with the behavior in the iron pnictides. In the case of FePn, a structural phase transition is either concomitant with or immediately prior to an AFM phase transition. The presence of ferro-orbital ordering of the $d_{xz,yz}$ states is intimately linked to the FePn structural phase transitions. Furthermore, iron-pnictide ferro-orbital ordering is associated with magnetic phase changes by virtue of spin-orbit coupling and Coulomb interaction. By contrast, the absence of ferro-orbital ordering in $La_2O_2Fe_2O(S,Se)_2$ may be due to the apparent non-degeneracy of the $d_{xz,yz}$ orbitals. [10]

VI. CONCLUSIONS

We have presented a comparison of the structural and magnetic properties of the homologues $La_2O_2Fe_2O(S,Se)_2$ based on bulk transport neutron powder diffraction data. Our motivation was to present a comparison of the structural details of M= S and Se as there had been no previously published, explicit comparison of these compounds. Neutron powder diffraction indicates that the structures of $La_2O_2Fe_2O(S,Se)_2$ are very similar with the main distinction being the difference in lattice size based on the atomic radii of the two chalcogens. Nuclear Bragg diffraction data indicates that the FeO_2Se_4 and FeO_2S_4 octahedra are distorted. This distortion is expected to be related to the presence of the relatively high extent of electron correlation compared to the iron pnictides. Structural distortion can be related to the absence of a structural phase transition. For example, distorted octahedra can diminish magnetoelastic coupling by precluding orbital ordering that is necessary to

establish a link between the magnetic phase transition and a structural phase transformation. Observing only a magnetic phase transition from the high-temperature paramagnetic phase to a lower temperature AF phase, we used group theory and magnetic refinement methods to determine the magnetic structure of these materials. 2D Ising symmetry was determined for both $La_2O_2Fe_2O(S,Se)_2$. We discussed models of frustrated magnetism and their relevance to metallic and insulating behavior iron based materials. Our results show the need to further understand how the magnetism of iron-based Mott insulators influences such material as they tuned near a metal-insulator boundary.

VII. AKNOWLEDGEMENTS

We are grateful to the technical staff at CNBC for excellent support. Work at Lawrence Berkeley National Laboratory and UC Berkeley was supported by the Office of Science, Office of Basic Energy Sciences (BES), Materials Sciences and Engineering Division of the U.S. Department of Energy (DOE) under Contract No. DE-AC02-05-CH1231 within the Quantum Materials Program (KC2202) and BES. The work at Zhejiang University was supported by the National Basic Research Program of China (973 Program) under Grants No. 2011CBA00103 and 2012CB821404, the National Science Foundation of China (No. 11374261, 11204059) and Zhejiang Provincial Natural Science Foundation of China (No. LQ12A04007). M.S.L thanks MPIPKS, Dresden for hospitality. L.C.'s work was supported by CNPq (Grant No. 307487/2014-8). L.C. also thanks the Physical Chemistry Department at Technical University Dresden for hospitality.

[1] C. Stock and E. E. McCabe, Journal of Physics: Condensed Matter **28**, 453001 (2016).

[2] G. Jin, Y. Wang, X. Dai, X. Ren, and L. He, Phys. Rev. B **94**, 075150 (2016).

[3] R. K. Oogarah, C. P. J. Stockdale, C. Stock, J. S. O. Evans, A. S. Wills, J. W. Taylor, and E. E. McCabe, Phys. Rev. B **95**, 174441 (2017).

[4] L. Craco, M. S. Laad, and S. Leoni, J. Phys.: Condensed Matter **26**, 145602 (2014).

[5] J.-X. Zhu, R. Yu, H. Wang, L. L. Zhao, M. D. Jones, J. Dai, E. Abrahams, E. Morosan, M. Fang, and Q. Si, Phys. Rev. Lett. **104**, 216405 (2010).

[6] H. Lei, H. Ryu, V. Ivanovski, J. B. Warren, A. I. Frenkel, B. Cekic, W.-G. Yin, and C. Petrovic, Phys. Rev. B **86**, 195133 (2012).

[7] S. Landsgesell, K. Proke, C. Colin, D. Abou-Ras, and N. Schfer, Journal of Superconductivity and Novel Magnetism **28**, 1111 (2015).

[8] J. M. Mayer, L. F. Schneemeyer, T. Siegrist, J. V. Waszczak, and B. Van Dover, Angewandte Chemie International Edition in English **31**, 1645 (1992).

[9] M. Dzero, K. Sun, V. Galitski, and P. Coleman, Phys. Rev. Lett. **104**, 106408 (2010).

[10] B. Freelon, Y. H. Liu, J.-L. Chen, L. Craco, M. S. Laad, S. Leoni, J. Chen, L. Tao, H. Wang, R. Flauca, Z. Yamani, M. Fang, C. Chang, J.-H. Guo, and Z. Hussain, Phys. Rev. B **92**, 155139 (2015).

[11] A. V. Chubukov, D. V. Efremov, and I. Eremin, Phys. Rev. B **78**, 134512 (2008).

[12] Y. T. M. Imada, A. Fujimori, Rev. Mod. Phys. **70**, 1039 (1998).

[13] T.-P. Choy and P. Phillips, Phys. Rev. Lett. **95**, 196405 (2005).

[14] G. S. Boebinger, Y. Ando, A. Passner, T. Kimura, M. Okuya, J. Shimoyama, K. Kishio, K. Tamasaku, N. Ichikawa, and S. Uchida, Phys. Rev. Lett. **77**, 5417 (1996).

[15] K. Semba and A. Matsuda, Phys. Rev. Lett. **86**, 496 (2001).

[16] J. W. Simonson, K. Post, C. Marques, G. Smith, O. Khatib, D. N. Basov, and M. C. Aronson, Phys. Rev. B **84**, 165129 (2011).

[17] H. Zhang, X. Wu, D. Li, S. Jin, X. Chen, T. Zhang, Z. Lin, S. Shen, D. Yuan, and X. Chen, Journal of Physics: Condensed Matter **28**, 145701 (2016).

[18] Y. Fuwa, T. Endo, M. Wakeshima, Y. Hinatsu, and K. Ohoyama, Journal of the American Chemical Society **132**, 18020 (2010).

[19] D. G. Free, N. D. Withers, P. J. Hickey, and J. S. O. Evans, Chemistry of Materials **23**, 1625 (2011).

[20] H. Lei, E. S. Bozin, A. Llobet, V. Ivanovski, V. Koteski, J. Belosevic-Cavor, B. Cekic, and C. Petrovic, Phys. Rev. B **86**, 125122 (2012).

[21] S. Landsgesell, E. Blumenrther, and K. Proke, Journal of Physics: Condensed Matter **25**, 086004 (2013).

[22] Y. Liu, S. Zhang, W. Lu, L. Li, S. Tan, B. Yuan, J. Chen, and Y. Sun, Journal of Alloys and Compounds **618**, 263 (2015).

[23] S. Landsgesell, K. Proke, T. Hansen, and M. Frontzek, Acta Materialia **66**, 232 (2014).

[24] H. Kabbour, E. Janod, B. Corraze, M. Danot, C. Lee, M.-H. Whangbo, and L. Cario, Journal of the American Chemical Society **130**, 8261 (2008).

[25] E. E. McCabe, C. Stock, J. L. Bettis, M.-H. Whangbo, and J. S. O. Evans, Phys. Rev. B **90**, 235115 (2014).

[26] E. E. McCabe, D. G. Free, B. G. Mendis, J. S. Higgins, and J. S. O. Evans, Chemistry of Materials **22**, 6171 (2010).

[27] E. E. McCabe, D. G. Free, and J. S. O. Evans, Chem. Commun. **47**, 1261 (2011).

[28] J. B. He, D. M. Wang, H. L. Shi, H. X. Yang, J. Q. Li, and G. F. Chen, Phys. Rev. B **84**, 205212 (2011).

[29] J. Rodriguez-Carvajal, Physica B: Condensed Matter **192**, 55 (1993).

[30] D. G. Free and J. S. O. Evans, Phys. Rev. B **81**, 214433 (2010).

[31] Y. Fuwa, M. Wakeshima, and Y. Hinatsu, Journal of Physics: Condensed Matter **22**, 346003 (2010).

[32] Y. Fuwa, M. Wakeshima, and Y. Hinatsu, Solid State Communications **150**, 1698 (2010).

[33] D. Charkin, V. Plotnikov, A. Sadakov, O. Omelyanovskii, and S. Kazakov, Journal of Alloys and Compounds **509**, 7344 (2011).

[34] A. Wills, Physica B: Condensed Matter **276**, 680 (2000).

[35] J. Rodríquez-Carvajal and T. Roisnel, in *European Powder Diffraction EPDIC 7*, Materials Science Forum, Vol. 378 (Trans Tech Publications, 2001) pp. 118–123.

[36] E. E. McCabe, C. Stock, E. E. Rodriguez, A. S. Wills, J. W. Taylor, and J. S. O. Evans, Phys. Rev. B **89**, 100402 (2014).

[37] S. D. Wilson, Z. Yamani, C. R. Rotundu, B. Freelon, E. Bourret-Courchesne, and R. J. Birgeneau, Phys. Rev. B **79**, 184519 (2009).

[38] Kazumasa Horigane, Kenji Kawashima, Sungdae Ji, Masaaki Yoshikawa, Despina Louca, and Jun Akimitsu, in *Proceedings of the International Conference on Strongly Correlated Electron Systems (SCES2013)*, JPS Conference Proceedings, Vol. 3 (Journal of the Physical Society of Japan, 2014).

[39] W. Lv, J. Wu, and P. Phillips, Phys. Rev. B **80**, 224506 (2009).

[40] M. Günther, S. Kamusella, R. Sarkar, T. Goltz, H. Luetkens, G. Pascua, S.-H. Do, K.-Y. Choi, H. D. Zhou, C. G. F. Blum, S. Wurmehl, B. Büchner, and H.-H. Klauss, Phys. Rev. B **90**, 184408 (2014).

[41] Y. Liu, S. Zhang, S. Tan, B. Yuan, X. Kan, L. Zu, and Y. Sun, J. Sol. State Chem. **221**, 272 (2015).

[42] J. Kanamori, Prog. of Theo. Phys. **17**, 177 (1957).

[43] Q. Si, R. Yu, and E. Abrahams, Nat. Rev. Mater. **1**, 16017 (2016).

[44] P. Bilbao Ergueta and A. H. Nevidomskyy, Phys. Rev. B **92**, 165102 (2015).

[45] S.-S. Gong, W. Zhu, D. N. Sheng, and K. Yang, Phys. Rev. B **95**, 205132 (2017).

[46] R. Yu and A. H. Nevidomskyy, Journal of Physics: Condensed Matter **28**, 495702 (2016).

[47] M. Wang, P. Valdivia, M. Yi, J. X. Chen, W. L. Zhang, R. A. Ewings, T. G. Perring, Y. Zhao, L. W. Harriger, J. W. Lynn, E. Bourret-Courchesne, P. Dai, D. H. Lee, D. X. Yao, and R. J. Birgeneau, Phys. Rev. B **92**, 079901 (2015).